iScience

CellPress
OPEN ACCESS

Article

Night vision restored in days after decades of congenital blindness

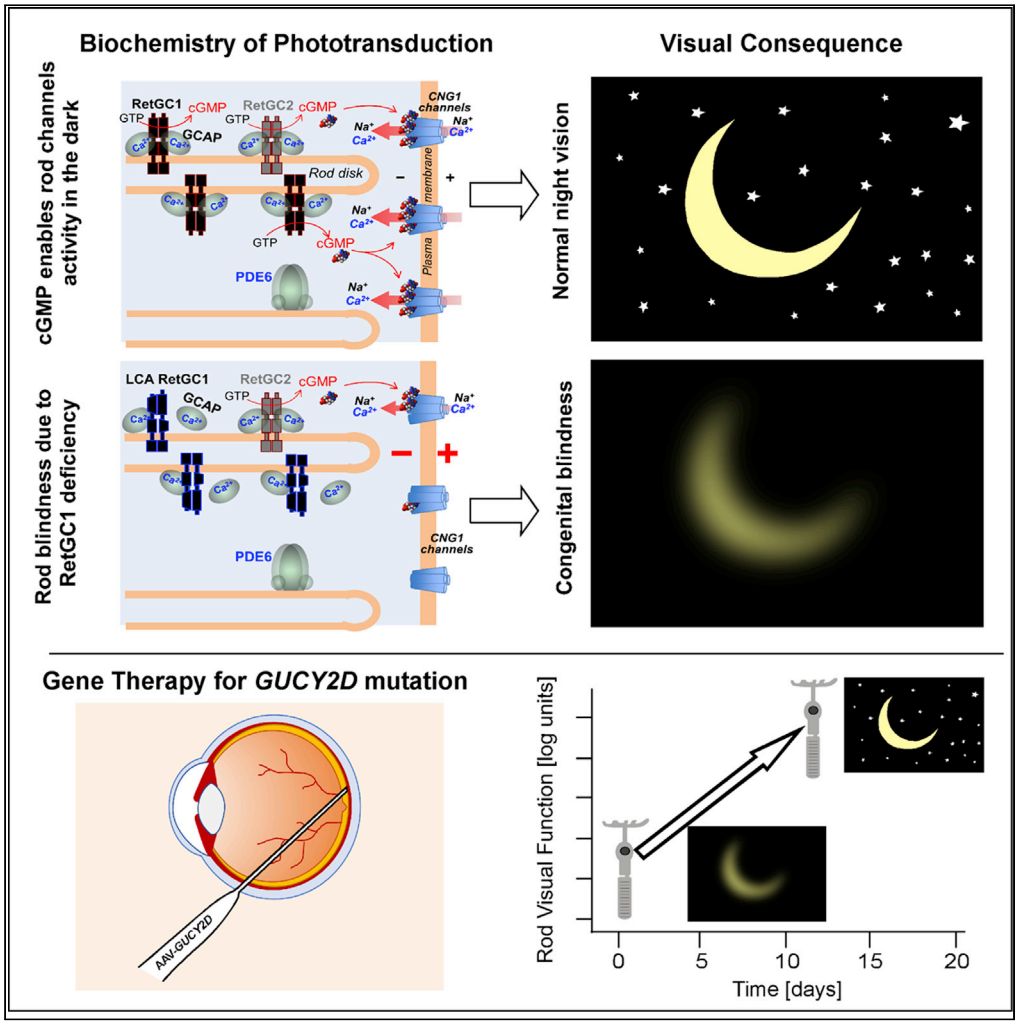

Samuel G. Jacobson, Artur V. Cideciyan, Allen C. Ho, ..., Igor V. Peshenko, Alexander M. Dizhoor, Shannon E. Boye

sjacobso@pennmedicine.upenn.edu

Highlights

Phototransduction, the biochemical cascade in photoreceptors, initiates vision

Congenital blindness can be due to defective phototransduction (*GUCY2D* gene mutations)

GUCY2D gene therapy (low dose) suggested some efficacy after months post-treatment

Higher dose therapy now shows log units of improved night (rod) vision over days

Jacobson et al., iScience *25*, 105274
October 21, 2022
https://doi.org/10.1016/j.isci.2022.105274

iScience

CellPress
OPEN ACCESS

Article

Night vision restored in days after decades of congenital blindness

Samuel G. Jacobson,[1,7,*] Artur V. Cideciyan,[1] Allen C. Ho,[2] Alejandro J. Roman,[1] Vivian Wu,[1] Alexandra V. Garafalo,[1] Alexander Sumaroka,[1] Arun K. Krishnan,[1] Malgorzata Swider,[1] Abraham A. Mascio,[1] Christine N. Kay,[3] Dan Yoon,[3] Kenji P. Fujita,[3] Sanford L. Boye,[4] Igor V. Peshenko,[5] Alexander M. Dizhoor,[5] and Shannon E. Boye[6]

SUMMARY

Signaling of vision to the brain starts with the retinal phototransduction cascade which converts visible light from the environment into chemical changes. Vision impairment results when mutations inactivate proteins of the phototransduction cascade. A severe monogenically inherited blindness, Leber congenital amaurosis (LCA), is caused by mutations in the *GUCY2D* gene, leading to a molecular defect in the production of cyclic GMP, the second messenger of phototransduction. We studied two patients with *GUCY2D*-LCA who were undergoing gene augmentation therapy. Both patients had large deficits in rod photoreceptor-based night vision before intervention. Within days of therapy, rod vision in both patients changed dramatically; improvements in visual function and functional vision in these hyper-responding patients reached more than 3 $\log_{10}$ units (1000-fold), nearing healthy rod vision. Quick activation of the complex molecular pathways from retinal photoreceptor to visual cortex and behavior is thus possible in patients even after being disabled and dormant for decades.

INTRODUCTION

Phototransduction, a G-protein-mediated signaling pathway, is the biochemical cascade in photoreceptors that is activated when light is absorbed by visual pigments. Activation steps of the cascade proceed to amplification and then to an electrical response (Lamb, 2022). For vision to occur, there needs to be opening and closure of cGMP-gated channels, controlled by multiple proteins that define the excitation and the recovery phases of the electrical response. Proteins of phototransduction pathways have been identified and mutations in the genes encoding the proteins are now known to be associated with genetic retinal diseases (Wright et al., 2010).

GUCY2D encodes retinal guanylyl cyclase 1 (RetGC1) (Dizhoor et al., 1994; Lowe et al., 1995), a key enzyme that allows for maintaining cGMP-gated electric current in the dark and accelerates the recovery phase of the photoresponse, thereby readying the biochemical process to recycle. Based on animal studies, RetGC1 is one of two RetGC isozymes, RetGC1 and RetGC2, present in mammalian photoreceptors (Dizhoor and Peshenko, 2021; Lowe et al., 1995). Guanylyl cyclase deficiency has been genetically engineered in mice in order to understand the pathophysiology and to model the severe congenital human blindness Leber congenital amaurosis (LCA) caused by biallelic recessive mutations in the *GUCY2D* gene (Baehr et al., 2007; Boye, 2016; Perrault et al., 1996; Yang et al., 1999). The human disease, historically considered untreatable and incurable, differs from other forms of LCA in that there is a preserved photoreceptor nuclear layer across a wide expanse of rod-rich retina with some cell loss mainly in the central foveal (cone-rich) region (Jacobson et al., 2013, 2016, 2017). The presence of intact rod photoreceptor structure in regions of impaired rod vision led to the hypothesis that a gene therapy strategy would be warranted. Unknown, however, was whether the photoresponse could be restored in RetGC1-deficient rods after decades-long dysfunction of their cGMP-gated channels.

Our previous report of the first cohort of patients with *GUCY2D*-LCA treated with gene augmentation (lowest dose administered, 3.3×10^{10} vg/mL) provided evidence of improved rod photoreceptor-mediated vision in two of three patients (Jacobson et al., 2021). Rod function improvement of ~1 log unit (l.u.) was detected between 30 and 60 days post treatment, as assessed with full-field stimulus testing

[1]Scheie Eye Institute, Department of Ophthalmology, Perelman School of Medicine, University of Pennsylvania, Philadelphia, PA 19104, USA

[2]Wills Eye Hospital, Thomas Jefferson University, Philadelphia, PA 19107, USA

[3]Atsena Therapeutics, Inc., Durham, NC 27709, USA

[4]Department of Pediatrics, Powell Gene Therapy Center, University of Florida College of Medicine, Gainesville, FL 32601, USA

[5]Pennsylvania College of Optometry, Salus University, Elkins Park, PA 19027, USA

[6]Department of Pediatrics, Division of Cellular and Molecular Therapy, University of Florida College of Medicine, Gainesville, FL 32611, USA

[7]Lead contact

*Correspondence: sjacobso@pennmedicine.upenn.edu

https://doi.org/10.1016/j.isci.2022.105274

(FST) (Roman et al., 2007). Like many patients with *GUCY2D*-LCA (Jacobson et al., 2017), the two responders at baseline had substantial rod function (within 1.8 l.u.. of normal). The statistically significant rod improvement, detected even with this large baseline level of rod activity, prompted the hypothesis that the rod photoreceptor should be seriously considered as the main target for this gene augmentation. To test this hypothesis, we were able to study two patients with *GUCY2D*-LCA who at baseline had profoundly impaired rod visual function; these patients were in a cohort being treated with a high dose of 3.3×10^{11} vg/mL. Nine complementary methods were used to measure different aspects of photoreceptor-mediated vision. By 8–12 days post treatment, rod visual improvement was detectable by FST (Roman et al., 2007) and visually guided behavior (Roman et al., 2022a). Between 15 days and 3 months post treatment, rod improvement reached more than 3 l.u..; two perimetric methods (Cideciyan et al., 2021a) localized the efficacy to the retinal region targeted with subretinally delivered vector-gene. Low-luminance visual acuities showed large improvements in spatial vision; and pupillary light reflexes (Cideciyan et al., 2021a) provided objective evidence to support changes in light sensitivity.

RESULTS

Evidence of increased rod sensitivity within days after treatment

P1 and P2, two patients with *GUCY2D*-LCA (genotype and subject details in Table S1) received uniocular subretinally injected AAV5-*GUCY2D*. We measured sensitivities serially in each eye of P1 and P2 in the dark-adapted state with chromatic stimuli using FST, a tabletop ganzfeld stimulator used for psychophysical thresholds in LCA studies (Roman et al., 2007). At baseline, both eyes of P1 were symmetric and showed losses of rod sensitivity greater than 5.4 l.u. compared to healthy eyes. Similarly, both eyes of P2 were symmetric and showed rod sensitivity losses of 4.2 l.u.. All subsequent measures post treatment are provided as change from these baselines. In the untreated control eye of P1, at 3, 8, 12, and 14 days and 1, 2, and 3 months post treatment, there was no change (Figure 1A). Similarly, the control eye of P2 showed no difference in serial measures over 3 months. In the treated study eye of P1, there was a ~2 l.u. increase from baseline in light sensitivity that was rod-mediated and first detected at day 8. By 2 months, the rod increase had reached greater than 4.6 l.u. (Figure 1A, left). The study eye of P2 also showed a detectable increase in rod-mediated sensitivity at day 8 which continued to improve over 3 months of follow-up, reaching 3.1 l.u. at 3 months (Figure 1A, right), nearing 0.6 l.u. of the lower bound of normal.

To confirm and extend the FST results, we developed a novel method for measuring dark-adapted functional vision (Roman et al., 2022a) and this was performed in each eye of P1 and P2 with the contralateral eye patched (Figure 1B). At pre-treatment baseline (Pre), P1 showed substantially elevated mobility task thresholds (5.5 and 5.6 l.u. from normal median) for control and study eyes, respectively. In the study eye of P1, there were increasingly greater improvements in mobility threshold after treatment ranging from 2.7 l.u. at D12 to 4.4 l.u. at M3. There were no such improvements in the control eye. P2 did not have baseline testing: the earliest recordings in this patient were at M1 when the threshold for the control eye was 6.6 l.u. As the other metrics (FST and dark-adapted perimetry) performed in P2 before treatment clearly indicate symmetry between eyes ($p = 0.57$, FST and $p = 0.4$, perimetry; t-test) and were stable from baseline to M1 in the control eye ($p = 0.1$ and $p = 1$), P2's mobility thresholds at baseline in both eyes were imputed to be equal to the value recorded at M1 in the control eye. In the study eye of P2, mobility threshold was 2.3 l.u. at M1 and increased to 1.0 at M3, approaching the lower bound of normal (0.7 l.u.). In terms of inter-ocular difference, the study eye of P1 showed increasingly better performance ranging from 3.9 L.u. at M1 to 4.6 l.u. at M3. The study eye of P2 also showed increasingly better performance ranging from 4.3 l.u. at M1 to 5.6 l.u. at M3. Mobility performance thresholds were highly correlated with FST thresholds (Pearson's $r = 0.9$, $p < 0.001$).

We inquired whether these results were noticed by the two subjects in daily life by asking the following question: "Since you started this study, have you had any changes in vision?" P1 at M1 replied that "night vision is better since the surgery … can now make out objects in (my) room at night." At M2, P1 described "improved night vision and … can make out objects and people in the dark." P2 at M1 replied that "as the light gets dimmer, (I have) some night vision". At M3, P2's answer was: "… have improved night vision … dim lighting gives more contrast and ability to discern details for big objects."

Localization of the post-treatment difference in light sensitivity

The retinal location of the improved vision was identified with two forms of perimetry. P1 and P2 had sufficient stability of fixation to permit serial measurements of dark-adapted thresholds by chromatic

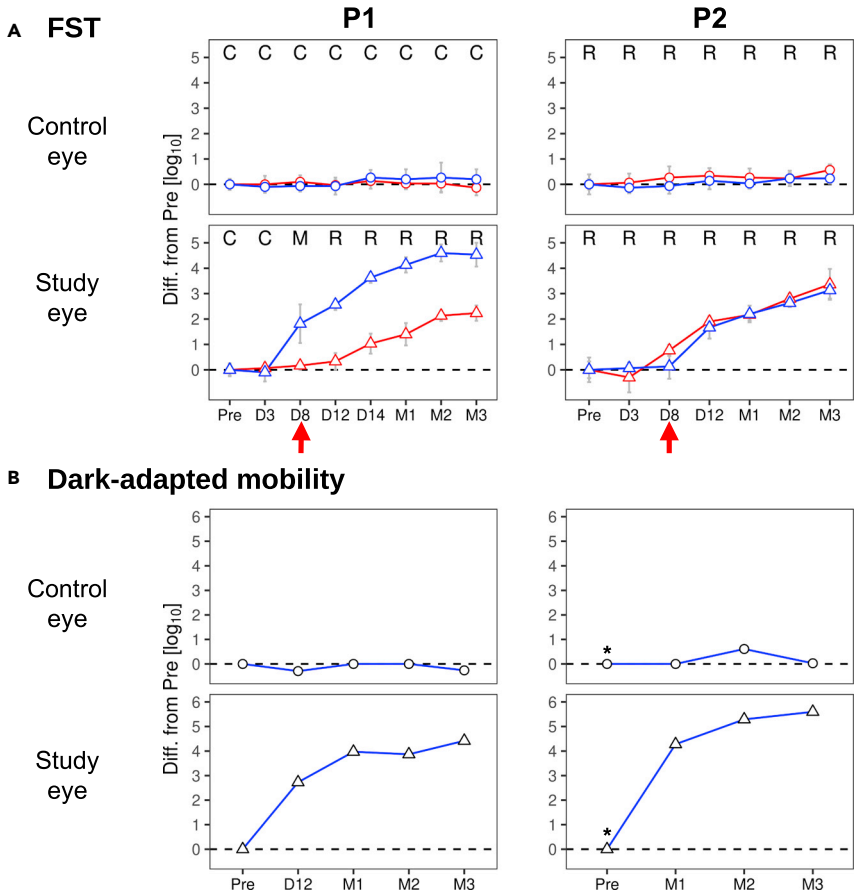

Figure 1. Time course of improvement in visual function and functional vision after treatment in two *GUCY2D*-LCA patients

(A) FST sensitivity for blue and red stimuli (blue and red lines and symbols, respectively) measured at pre-treatment baseline (Pre) and at subsequent timepoints post-treatment. Top row, circles: control eye; bottom row, triangles: study eye. R, M, C: rod, cone or mixed (rod detecting blue and cone detecting red stimuli) photoreceptors, respectively, mediating perception. Vertical red arrows: earliest time with noticeable post-treatment rod sensitivity increase. Rod sensitivity increases (from Pre) at latest time point in the study eye were >4.6 log units (l.u.) for P1 and 3.1 l.u. for P2, respectively. Dashed line: no change level; error bars: $\pm$2SD from multiple measurements, n $\geq$ 6.

(B) Thresholds for successful performance of a mobility task measured before treatment (Pre) and post-treatment. When using the control eye both patients required luminances >5.5 l.u. above normal for successful navigation which did not change after treatment (circles). In contrast, when using the study eye (bottom row) P1 (left) showed functional increases after treatment of 2.7 l.u. to 4.4 l.u. (triangles) compared to Pre. The study eye of P2 (right) showed functional increases after treatment of 4.3 l.u. to 5.6 l.u. (triangles) compared to Pre. These increases brought the functional vision threshold for the study eye within 1 L.u of the normal median threshold. (*), baseline of P2 imputed from value at M1 in the control eye.

perimetry (Figure 2A) and retina-tracking perimetry (also known as microperimetry) (Figure 2B). The two forms of perimetry have different advantages and provide partially independent evidence. Chromatic perimetry has a wide dynamic range and provides identity of the functioning photoreceptors. P1 at baseline had cone-mediated vision at all tested loci along the vertical meridian of both eyes (Figure 2A). At the next recording, day 11 post treatment, there was an increase in sensitivity of about 3 l.u. at loci between 15° and 30° in the inferior visual field and at a more central locus a few degrees inferior to fixation. By 15 days post treatment, the visual area extending from near fixation to 30° in the inferior field became contiguous with increased sensitivity of 3–4 l.u. higher than baseline. A further increase in sensitivity was observed at M1, M2, and also M3, with sensitivities 4 to 6 l.u. above baseline, approaching the lower limit of normal in some locations. All cone-mediated loci in the inferior field had now become mixed- (meaning rod and cone) or rod-mediated; the superior field remained mostly mixed- or cone-mediated. P2 at

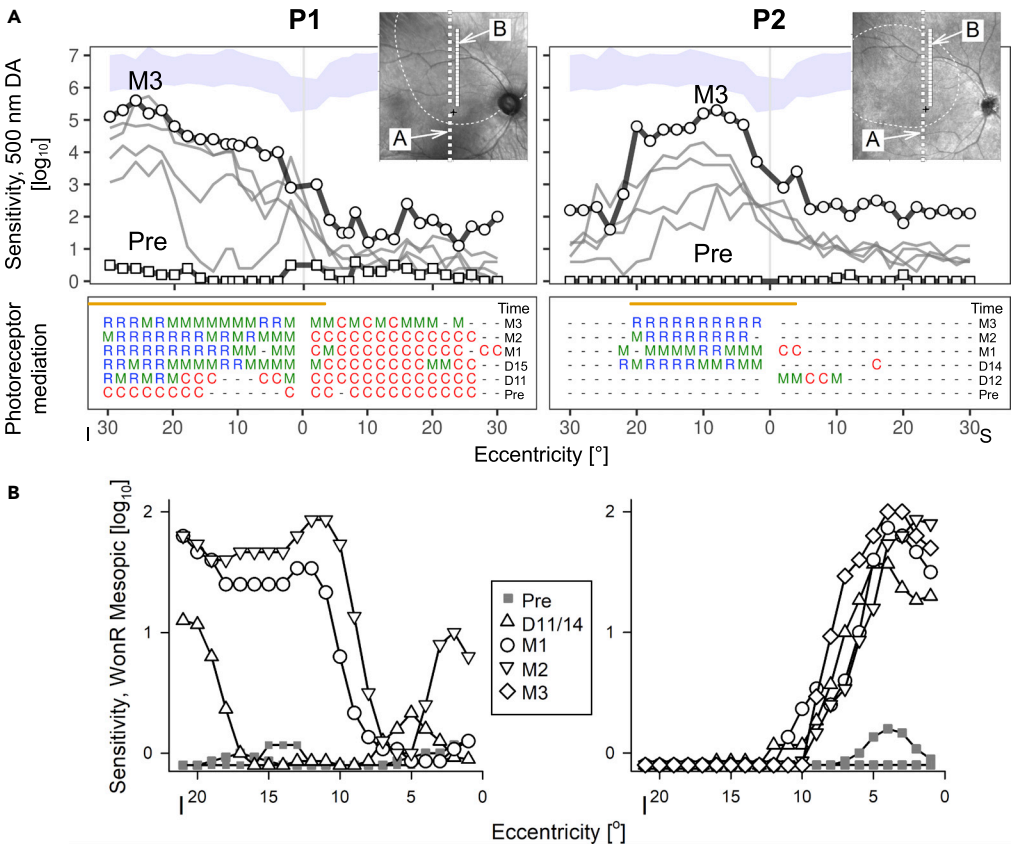

Figure 2. Localizing the efficacy

(A) Dark-adapted sensitivities to a 500 nm target across a vertical profile centered at the fovea, in study eyes pre- and post-treatment (days 11 to M3 for P1, and day 12 to M3 for P2). An increase in sensitivity co-located with the injection bleb (orange line shows extent along vertical median) is evident (top). Bottom, photoreceptor mediation (C, R, M for cone, rod and mixed rod/cone, respectively; dashes: mediation unable to be determined due to floor effect). The time sequence indicates the appearance of rod mediation after treatment. Squares, Pre; circles, latest visit; I, inferior; S, superior visual field.

(B) Microperimetry measurements of sensitivity to white stimuli on a dim red mesopic background as a function of eccentricity in the inferior field. Loci where the brightest available stimulus was not seen are plotted below the 0 dB line. Insets, NIR reflectance images overlaid with the loci tested (white squares) with perimetry (A) and microperimetry (B), the location of the injection bleb (white dashed lines), and the anatomical fovea (black cross).

baseline had no detectable sensitivities. Between 12 days and 3 months post treatment, the inferior field showed detectable sensitivities and these were now mixed- or rod-mediated. The increase in sensitivity across the 4° to 20° area in the inferior field was at least 4 to 5 l.u. higher than baseline, approaching within 0.7 l.u. of the lower bound of normal.

Retina-tracking mesopic microperimetry dynamically anchors to retinal features in eyes with nystagmus and was used to confirm the exact retinal localization of the changes in light sensitivity with respect to the location of the treatment. At two separate visits pre-injection, the brightest available (0 dB) stimulus was not seen by P1 and P2 at the great majority of loci tested (Figure 2B). At day 14 post injection in P1, there was a small increase in sensitivity near 5° eccentric, and a large increase in sensitivity starting at 18° eccentric in the superior retina. By M1, sensitivity improved further and extended centrally to cover most of the injection bleb; further increases were measured at M2 and M3. Similarly in P2, starting at day 11 after the injection and extending through M3, there was a large increase in sensitivity from 1° to 10° eccentricity in the superior retina that tended to expand over time. The lack of exact duplication between free viewing perimetry and microperimetry results may be partially explained with the scotopic versus mesopic test conditions and the existence of a ceiling effect in microperimetry due to stimulus dynamic range being limited to 2 l.u.

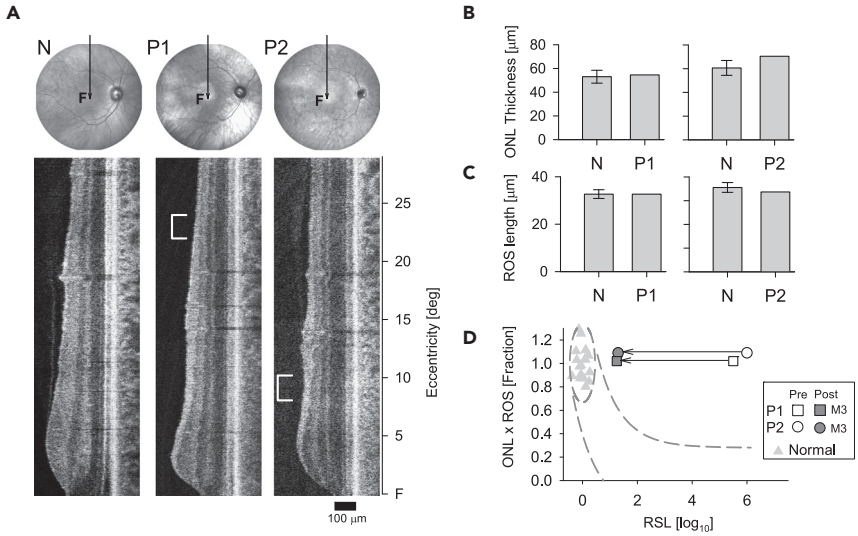

Figure 3. Retinal structure before treatment and structure-function relationship

(A) Fundus images (near-infrared) and OCT scans along the vertical meridian through the fovea of a normal subject (N), and patients 1 and 2 (P1, P2) before treatment. Scan position depicted by the arrow on fundus images; F, fovea. White brackets to the left side of the patient scans delimit the location of the peak sensitivity gained after treatment (500 nm, DA, Figure 2A) at 22–24° superior retina for P1 and 8°–10° superior retina for P2.

(B and C) Bar graphs are measurements of ONL (outer nuclear layer) thickness and ROS (rod outer segment) length at the location corresponding to post-treatment peak sensitivity (marked by brackets on the scans) and average normal value (N) at the same location (n = 13, error bar, SD).

(D) The relationship between photoreceptor layer structure and rod sensitivity loss (RSL) at the marked location in P1 and P2. Open symbols are RSL before treatment and filled symbols (dark gray) after 3 months (M3) post-treatment in P1 and P2. The ellipse encircling normal data (gray triangles) describes normal variability. Dashed lines represent the idealized model of the relationship between structure and function.

Changes to visual acuity

Visual acuity as measured with standardized ETDRS methods can show a very large spectrum of severity in *GUCY2D*-LCA (Jacobson et al., 2013, 2017, 2021). At baseline, P1 showed relatively retained visual acuities of 0.66 and 0.72 logMAR in control and study eyes, respectively; P2 had symmetric visual acuities of 1.34 logMAR. Post-operatively, visual acuity changes were within 0.12 logMAR in the control and study eyes of both patients. The results of low-luminance visual acuity (LLVA), however, were very different. At baseline, both patients could not correctly identify any LLVA letters implying an acuity equal or worse than 1.70 logMAR and low-luminance deficits of more than three lines. Post-operatively, in control eyes, there were small changes up to 8 letters (0.16 log). In study eyes, P1 improved by 45 letters (0.9) and P2 improved by 18 letters (0.36 log). LLVA improvements were likely driven by the large sensitivity improvements in the rod system of study eyes.

To evaluate potential changes to spatial vision driven by the long- and middle-wavelength (L/M−) sensitive cones, we measured grating acuities with red bars presented on a bright blue background (Cideciyan et al., 2016). Previous results in patients retaining healthy rods and short-wavelength sensitive cones support an L/M-cone-specific origin of this test method (Sumaroka et al., 2018). At baseline, P1 in both eyes could not distinguish the lowest contrast gratings, but with increasing contrast showed increasingly better spatial vision reaching 3.2 cyc/deg (1.0 logMAR) (Figure S1) which was substantially lower than the patient's ETDRS acuity. Post-operatively, there were no major changes in the control eye, but the study eye steadily improved in spatial vision across a range of lower contrast targets (Figure S1). P2 could not see any of the gratings at any point in either eye.

Is retinal structure normal prior to intervention?

As previously shown, patients with *GUCY2D*-LCA can have normal or near normal pericentral-peripheral retinal photoreceptor outer nuclear layer (ONL) thickness and deep outer retinal structure that is also within normal limits (Jacobson et al., 2013, 2017, 2021). Specifically, in these two patients, we measured (at

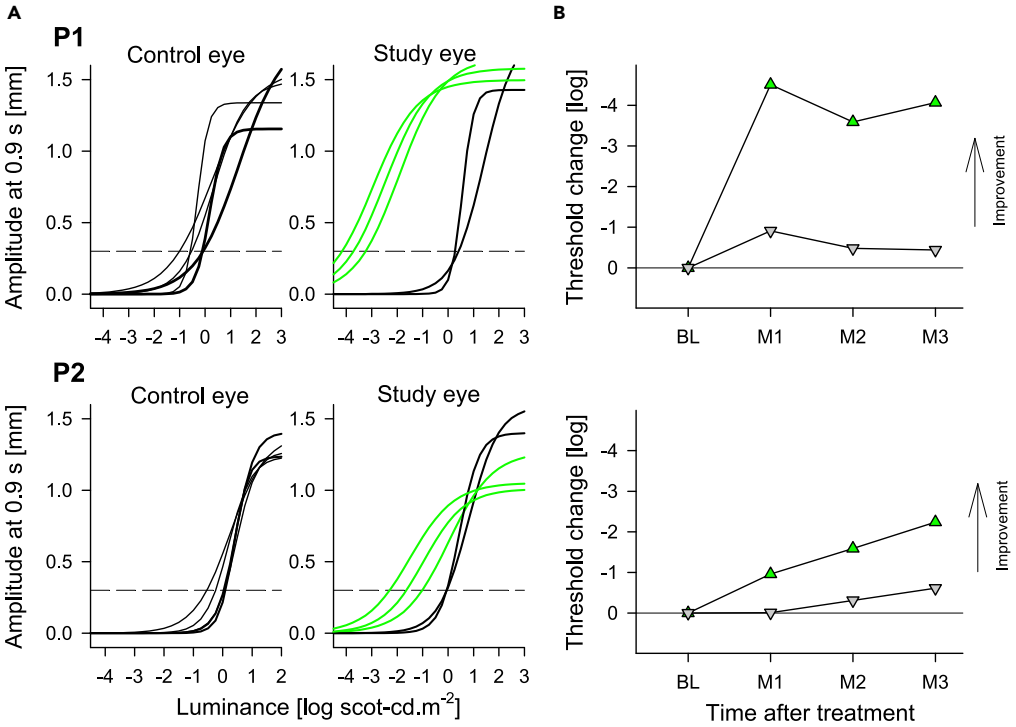

Figure 4. Dark-adapted pupillary light reflexes in patients P1 and P2 at baseline and post-operative visits

(A) Non-linear functions best fit to pupillary response amplitudes measured at 0.9 s after the start of 1 s long stimuli over a 6 log unit dynamic range of luminances presented to dark-adapted eyes. Thicker lines represent the pre-treatment time points, thinner black and green lines represent the post-treatment time points in untreated (control) and treated (study) eyes, respectively. Horizontal dashed lines demarcate criterion amplitude of 0.3 mm used to define response thresholds. (B) Change in response threshold from average pre-treatment values. Green up-triangles are treated study eyes; gray down-triangles are untreated control eyes. BL, baseline, M, month.

baseline) photoreceptor layer thickness in the region that was treated. ONL and rod outer segment (ROS) thickness measurements were normal (Figures 3A–3C) suggesting there was rod photoreceptor integrity in these regions. Co-localized rod visual function, however, was severely abnormal. As shown in our previous studies of patients with *GUCY2D*-LCA, this is an example of dissociation of structure and function and represents a theoretical possibility to increase rod vision, given therapy of the underlying cause (Jacobson et al., 2013, 2017). Measurements of function, however, have not been able to be made previously to test this hypothesis in patients with *GUCY2D*-LCA.

The characterization of *GUCY2D*-LCA as a disease with dissociation of structure and function is based on modeling of the relationship between photoreceptor layer structural parameters at a specific retinal location and the measured rod visual function at that location (Cideciyan and Jacobson, 2019; Jacobson et al., 2005). In the graph of this relationship (Figure 3D), normal variability is described by an ellipse encircling the 95% confidence interval of a bivariate Gaussian distribution. Dashed lines define the idealized model of the relationship between structure and function in pure photoreceptor degenerations and the region of uncertainty that results by translating the normal variability along the idealized model. Whereas photoreceptor structure was normal pre-treatment in P1 and P2, co-localized rod visual sensitivity was reduced by 5–6 log units. Measurements made at 3 months post treatment showed a dramatic improvement of rod sensitivity by ~4–5 log units. P1 and P2 are thus behaving post-treatment as predicted from these models.

Is there objective evidence of changes in visual function?

Once the magnitude of the improvement perceived by the subjects was defined by FST, retinally localized to the treated regions by perimetry, and consequences to functional vision quantified by dark-adapted mobility, we used pupillary reflexes to evaluate objective evidence for changes (Figure 4). Average pupillary response thresholds to stimuli pre-operatively were 0.13 and +0.01 log scot-cd.m^{-2} for P1 and P2,

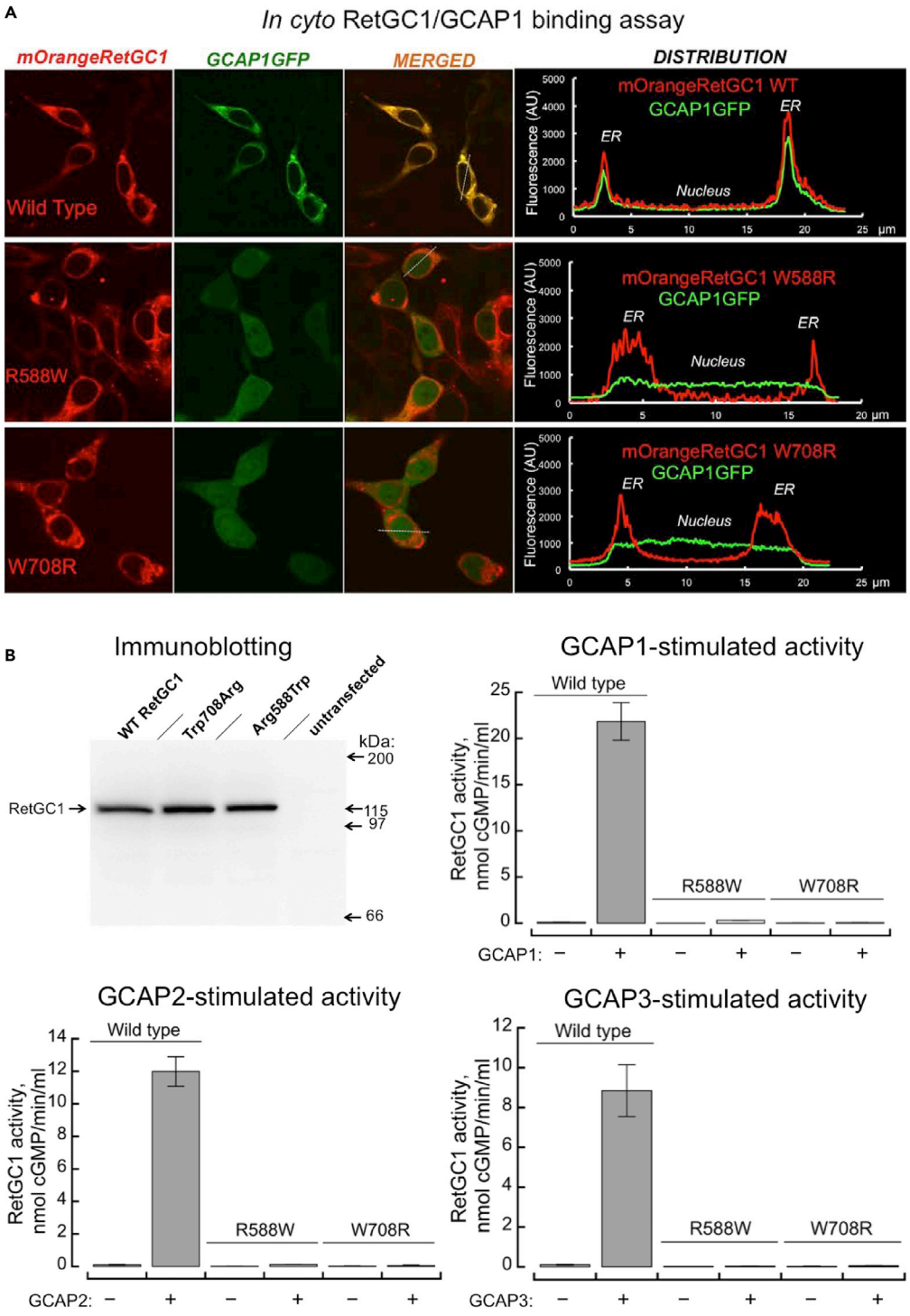

Figure 5. Biochemical consequences of *GUCY2D*-LCA missense mutations in patients P1 and P2

(A) *In cyto* co-localization of RetGC1 mutants with GCAP1. The cDNA coding for RetGC1 tagged with mOrange fluorescent protein (red) replacing a part of RetGC1 ECD are co-expressed in HEK293 cells with bovine GCAP1 harboring enhanced GFP tag at the C-terminus (green). The rightmost panel in each row presents typical distribution of the fluorescence intensities for the two fluorochromes across the cell (scanned along the dashed lines in the cells shown in the 'merged' images). Upper row, wild type RetGC1; middle row, Arg588Trp; bottom row, Trp708Arg. GCAP1GFP

Figure 5. *Continued*
fluorescence co-localizes with wild type RetGC1 in the ER membranes, but it fails to co-localize with Arg588Trp or Trp708Arg RetGC1 and remains uniformly distributed throughout the cytoplasm and the nucleus.
(B) Full-length wild type, Arg588Trp, and Trp708Arg RetGC1 expression in HEK293 cells was verified by Western immunoblotting. The HEK293 membrane samples containing wild type RetGC1 (n = 9 to 11 measurements), Arg588Trp (n = 3 to 4), and Trp708Arg (n = 5 to 8) were assayed for guanylyl cyclase activity (mean average ±SD) by incubating them for 30 min at 30°C in the presence (+) or in the absence (–) of 20 μM GCAP1, GCAP2, or GCAP3.

respectively (Figure 4A). In control eyes, post-operatively there were no changes. In study eyes however, there were large improvements to light sensitivity with response thresholds moving to −3.71 and −1.65 log scot-cd.m^{-2} for P1 and P2, respectively (Figure 4A). Change from baseline showed maximal improvements greater than 4 l.u. in P1 and 2 l.u. in P2 (Figure 4B).

Changes in RetGC1 biochemical properties caused by the *GUCY2D*- LCA mutations in P1 and P2

RetGC1 (Dizhoor and Peshenko, 2021; Lowe et al., 1995) coded by a human *GUCY2D* gene is a homodimeric enzyme (Figure S2A), in which the two catalytic (CAT) domains together create the active site of the dimer, converting GTP to cGMP (Liu et al., 1997). In P1 and P2, one of the two LCA *GUCY2D* alleles in each patient codes for a full-length RetGC1 polypeptide harboring a single-residue substitution in the kinase homology domain (KHD)—Arg588Trp in P1 (Figure S2B) or Trp708Arg in P2 (Figure S2C). Since the CAT domain was unaffected in either case, these two mutants would be able to have the active site. Therefore, we tested their ability to bind guanylyl cyclase activating protein (GCAP) *in cyto* and to catalyze cGMP production *in vitro* (Figure 5).

In contrast to wild type, the intracellular domains in Arg588Trp and Trp708Arg RetGC1 were unable to bind GCAP1, the main activator of RetGC1 *in vivo* (Olshevskaya et al., 2012). When the mOrange-tagged RetGC1 variants were co-expressed with GCAP1GFP in HEK293 cells (Peshenko et al., 2015a, 2015b) (Figure 5A), Pearson's correlation coefficients for the distribution of Arg588Trp and Trp708Arg mOrange RetGC1 versus GCAP1GFP in this *in cyto* assay were 0.32 ± 0.17SD (n = 28) and 0.09 ± 0.17SD (n = 27), respectively, both below the threshold indicative of co-localization (Zinchuk and Zinchuk, 2008) and significantly different ($p < 0.0001$; ANOVA/Scheffe post hoc, alpha 0.01) from the wild type (0.93 ± 0.06SD; n = 22). Untagged full-length Arg588Trp and Trp708Arg RetGC1 expressed in HEK293 cells were also directly tested for enzymatic activity *in vitro* using saturating concentration of the recombinant human GCAP1, GCAP2, or GCAP3 (Figure 5B). Both Arg588Trp and Trp708Arg mutants were virtually inactive when compared with the wild type (<1.5% wild type activity; ANOVA/Sheffe $p < 0.0001$, alpha 0.01).

The second LCA allele in P1, Thr839fs, *a priori* lacks the ability to produce active RetGC1, because deletion of the second base in the codon 839 causes a frameshift and the aberrant sequence terminates 21 residues downstream of the resultant Arg839. The truncated Thr839fs mutant lacks CAT domain and therefore cannot form the active site, neither on its own, nor in combination with a full-length RetGC1subunit (Figure S2B). The second LCA allele, c.-148T>C, in P2 (Table S1, Figure S2C) does not alter RetGC1 protein sequence, but likely disables transcription of mRNA from this allele.

DISCUSSION

How do the current results relate to the literature on effects of abnormalities in the phototransduction cascade, specifically the effect of retinal guanylyl cyclase deficiency? A biochemical and physiological consequence has been proposed: cGMP would not be made; channels stay closed; and there would be reduced calcium influx (Baehr et al., 2007; Peshenko et al., 2011). This was thought to equate to chronic light exposure, and subsequent photoreceptor cell death (Fain, 2006; Karan et al., 2008). A naturally occurring chicken with a null mutation in the guanylyl cyclase gene showed early photoreceptor dysfunction followed by rapid retinal degeneration; the disease course was slowed by gene transfer (Boye, 2016; Semple-Rowland et al., 1998; Ulshafer et al., 1984; Williams et al., 2006). In contrast to the avian model, a mammalian animal model replicating deficiency of a murine ortholog of *GUCY2D* showed no significant degeneration of rods and only slow degeneration of cones (Yang et al., 1999). The model demonstrated that the lack of cGMP synthesis in the absence of RetGC1 is not complete—the ancillary RetGC2 isozyme unable to support normal photoresponses is still sufficient to keep rods alive and even support their response, albeit abnormal, to light (Baehr et al., 2007; Olshevskaya et al., 2012; Yang et al., 1999). Proof-of-concept gene

augmentation experiments in RetGC1 knockout mice mainly led to improved cone photoreceptor outcomes (Boye et al., 2010, 2011; Mihelec et al., 2011). A RetGC1/RetGC2 double knockout murine model did lead to both cone and rod photoreceptor dysfunction and degeneration; both rod and cone function were positively affected by gene therapy (Boye et al., 2013; Boye, 2014).

How closely do the animal models mirror the human disease expression of *GUCY2D*-LCA? In early studies that defined the molecular basis of LCA, the phenotype of *GUCY2D*-LCA (LCA1) was contrasted with that of *RPE65*-LCA (LCA2) (Perrault et al., 1999). LCA1 was characterized as a cone > rod dystrophy, while LCA2 was considered a rod > cone dystrophy. In recent years, we quantified rod and cone vision using FST in a cohort of patients with *GUCY2D*-LCA, and found different phenotypes within the LCA1 molecular group (Jacobson et al., 2017). In 24 patients studied, there was a spectrum of cone losses, but all were abnormal. Pertinent to the present study, the group we previously studied could be divided by rod losses. There were ~29% with severe rod vision disturbances (>3.5 log units); another ~42% had minimal to moderately abnormal rod losses (between >1–3.5 log units); a smaller percentage of patients (17%) had very limited rod loss (0.5–1 log units); and an even smaller percent (13%) had <0.5 log units of rod loss. Are such data consistent with the current literature? Two recent studies provided percentages of patients with *GUCY2D*-LCA with nyctalopia (not quantified) as a symptom: 38% (8/21) (Bouzia et al., 2020) and 7% (1/14 patients) (Hahn et al., 2022).

From a biochemical perspective, *GUCY2D*-LCA mutations cause severe reduction or a complete loss of RetGC1 biochemical activity (Jacobson et al., 2013, 2021; Peshenko et al., 2010). In line with that, a direct biochemical analysis shows that despite the preservation of the full-length RetGC1 primary structure, the single amino acid substitutions, Arg588Trp in P1 and Trp708Arg in P2, produce inactive RetGC1 lacking the ability to bind its activator protein, GCAP. Interestingly, the mutation causing Thr839fs substitution in P1, like another *GUCY2D*-LCA mutation Arg822Pro (Jacobson et al., 2013; Peshenko et al., 2015b), occurs in exon 13. This exon codes for the dimerization domain of RetGC1 and the adjacent parts of KHD and CAT domains. It is also known for harboring the mutations causing dominant cone-rod dystrophy CORD6 (or adCORD) (Sharon et al., 2018). The dimerization domain of RetGC1 is also essential for its regulation by GCAP1 (Peshenko et al., 2015b). The reason behind the different mutations in the dimerization domain causing clinically dissimilar disorders, CORD6 and LCA, is that different substitutions in the same domain can change biochemical properties of the cyclase in a profoundly different manner. The gain-of-function CORD6 mutations abnormally increase RetGC1 affinity for Mg^{2+} GCAP1 and therefore produce "phototransduction disease", abnormally elevating of cGMP and Ca^{2+} in the photoreceptor outer segment (Sato et al., 2018). In contrast, the LCA mutations in the same domain, such as Arg822Pro (Peshenko et al., 2015b), can cause loss of RetGC1 function by disrupting GCAP1 binding. In this study, the second LCA allele in P1, Thr839fs, truncates RetGC1 at the end of the dimerization domain and deletes the entire catalytic domain of the enzyme, rendering it *a priori* inactive (Figure S2B).

The effect of the −148T>C (Chr17:7,905,914 T>C, Patient P2) cannot be tested biochemically, because the protein coding sequence remains unchanged (Figure S2C). In the *GUCY2D* gene (NCBI Reference Sequence: NM_000180.4), this substitution is located 19 bp upstream from exon 1, infringing on the promoter region of the gene, and possibly disables its transcription in photoreceptors. Although very likely, this explanation cannot be directly verified using RetGC1 expression in HEK293, where RetGC1 cDNA is heterologously expressed under the control of a cytomegalovirus (CMV) promoter, not the presently uncharacterized photoreceptor-specific *GUCY2D* promoter.

When it comes to restoration of rod vision by *GUCY2D* gene augmentation therapy, the best candidates would probably be those patients whose mutations completely negate RetGC1 activity and/or activation by GCAPs *in vitro*, because increase of RetGC1 activity would be most beneficial for the rods that completely lack such activity. However, this criterion alone might not be fully sufficient for making the selection, because variability of the ancillary isozyme, RetGC2, expression between different patients could not be *a priori* excluded. A number of studies indicate that the genetic background of the patients with *GUCY2D*-LCA, along with the exact positions of the mutations, may play a role in clinical symptoms (Bouzia et al., 2020; Sharon et al., 2018). Visual function measurements of the degree of night vision loss in the patients themselves would be the primary guidance criterion for the prospective restoration of rod vision.

The complex effects of retinal guanylyl cyclase deficiency on rod photoreceptors led to the decision that the cell target for efficacy in a first-in-human RetGC1 gene augmentation clinical trial would be cone

photoreceptors. The emphasis by the FDA on improvement (by 3 ETDRS lines) of best-corrected visual acuity as a clinically meaningful efficacy endpoint also tended to weigh in favor of cones (Csaky et al., 2017). Unexpectedly, however, in the first cohort of our current gene therapy clinical trial, two of the three patients had statistically significant rod photoreceptor visual improvement (Jacobson et al., 2021). The gain in rod function was about 1 log unit and this was first detected 1–2 months post treatment. The caveats were that this was the lowest dose administered in the trial at that point, and the patients had substantial rod function at baseline (~2 log units from normal limits). Detection of rod efficacy signals in these first two patients led to the idea that rod photoreceptor function and rod phototransduction needed to be explored further in response to this gene augmentation, and that any subsequent patients with *GUCY2D*-LCA entering the trial with severely reduced rod vision at baseline deserved intense study. Two such patients enrolled in the clinical trial within the cohort receiving the highest dose allowed testing of our hypothesis from the cohort 1 observations.

The surprising speed of functional rod recovery in the patients with *GUCY2D*-LCA suggests that all the molecular machinery of phototransduction remains intact in RetGC1-deficient human rods retaining only the ancillary isozyme RetGC2, unlike the downregulation of some phototransduction proteins observed in RetGC1/RetGC2 double knockout mice (Baehr et al., 2007). A simple hypothesis is that, given intact molecular machinery, the time course may just be the rate of lengthening of rod outer segments disturbed by the induced retinal detachment for delivering the gene augmentation therapy, and the reapposition of the photoreceptors to the retinal pigment epithelium. Measurements of photoreceptor segments (outer + inner) length before and after surgery at the retinal site of peak rod visual improvement was possible in P1 and showed a shortening at day 3 but recovery thereafter (Figure S3) (Guérin et al., 1993; Nork et al., 2012; Young, 1971). There is the intriguing possibility that the rate of rod visual recovery may have been even faster if the postulated recovery from the known consequences of induced retinal detachment did not need to be factored in (Jacobson et al., 2012).

Has a rapid restoration of rod vision such as in *GUCY2D*-LCA been documented in any other early-onset blindness? There are limited human clinical trial results that have shown improvements to allow for a direct comparison to the current work. Gene therapy for *RPE65*-LCA shows large improvements in rod photoreceptor-mediated visual function (Jacobson et al., 2012; Maguire et al., 2021). By 1 month post injection, best-responding patients with *RPE65*-LCA have shown 2–4 l.u. of rod sensitivity improvement by chromatic dark-adapted FST (Jacobson et al., 2012) but the preceding time course of improvement has not been defined. Similarly, in a Phase 3 trial, patients with *RPE65*-LCA have shown 2–3 l.u. improvement in light sensitivity at 1 month post injection with white FST (Maguire et al., 2021), but photoreceptor origin and preceding time course were not defined. Because some patients with *RPE65*-LCA undergoing gene therapy had verbally reported localized increases in perceived brightness occurring as early as 7–10 days following injection (Cideciyan et al., 2008), we analyzed available data from our *RPE65*-LCA clinical trial (Table S2). Ten of 15 patients showed large rod-mediated increases in blue FST ranging from 0.9 to 2.4 l.u. (average 1.3 l.u.), first detectable between 5 and 30 days (average 14.2 days).

Extrapolating from the available evidence, it is parsimonious to conclude that AAV-vectored augmentation of key enzymes in the RPE (in *RPE65*-LCA) and in the rod photoreceptors (in *GUCY2D*-LCA) can demonstrate rapid activation with measurable improvements occurring within the first two weeks. How this rapid time course compares to improvements in cone photoreceptors with augmentation of enzymes, or in rod and/or cone improvements with augmentation of structural proteins remains to be evaluated. It is of note that reconstituting structural proteins in the foveal cone photoreceptor ciliary transition zone with an antisense oligonucleotide (in *CEP290*-LCA) appears to have a slower turn on (Cideciyan et al., 2021b).

In summary, the present results indicate that there can be remarkable gains in rod vision after gene augmentation in patients with *GUCY2D*-LCA. Both patients had profound rod dysfunction at baseline but structural evidence of rod photoreceptor integrity in the treated retinal region. Proof was provided that the increase in rod function was derived from the treated region. Quantitative evidence from multiple concordant measures (Table S3) suggests that a major effect of this AAV-*GUCY2D* (and this dose level) is on rod function and outcomes that quantify rod vision are a high priority. The reconstitution of rod-mediated vision suggests that rod photoreceptors are indeed surviving, that a decades-long singular molecular defect has not resulted in a major shift in expression of remaining molecular components driving the complex deactivation phase of phototransduction, and that the post-phototransduction visual pathways can be functionally restored.

Limitations of the study

This study is limited in the number of patients. This is due to the rarity of the disease and the number of total participants enrolled in this first-in-human clinical trial. The clinical trial is ongoing. Although enrollment is closed, the patients who are enrolled, including the two reported here, will be evaluated at future study timepoints.

STAR★METHODS

Detailed methods are provided in the online version of this paper and include the following:

- KEY RESOURCES TABLE
- RESOURCE AVAILABILITY
  - Lead contact
  - Materials availability
  - Data and code availability
- EXPERIMENTAL MODEL AND SUBJECT DETAILS
- METHOD DETAILS
  - Spatial vision
  - Full field stimulus testing (FST) – Chromatic, dark-adapted state
  - Mobility in the dark-adapted state
  - Dark-adapted chromatic perimetry
  - Retina-tracking mesopic microperimetry
  - Retinal structure - Optical coherence tomography
  - Pupillary light reflex (PLR)
  - Guanylyl cyclase expression and assays
- QUANTIFICATION AND STATISTICAL ANALYSIS
- ADDITIONAL RESOURCES

SUPPLEMENTAL INFORMATION

Supplemental information can be found online at https://doi.org/10.1016/j.isci.2022.105274.

ACKNOWLEDGMENTS

This work was supported by Atsena Therapeutics, Inc., and in part by grant EY11522 from National Eye Institute (A.M.D.) and CURE Formula grant from Pennsylvania Department of Health (A.M.D.).

AUTHOR CONTRIBUTIONS

S.G.J. and A.V.C. conceived and directed the study; collected, reviewed, analyzed and interpreted the data; and wrote the draft manuscript; A.C.H. performed the subretinal surgery; A.J.R., V.W., A.V.G., A.S., A.K.K., M.S., and A.A.M. collected and analyzed data; C.N.K., D.Y., and K.P.F. contributed to clinical aspects of the study; A.M.D. and I.V.P. conducted experiments (mutant RetGC expression and activity measurements) and analyzed the data. S.L.B. and S.E.B. provided data on the vector used in the study.

DECLARATION OF INTERESTS

S.E.B. and S.L.B. are scientific founders of and equity holders in Atsena Therapeutics, Inc. and are patent holders on the use of AAV-*GUCY2D* for the treatment of LCA1. C.N.K., D.Y., and K.P.F. are employees of Atsena Therapeutics, Inc. All other authors have no competing financial interests.

Received: July 12, 2022
Revised: August 29, 2022
Accepted: September 30, 2022
Published: October 21, 2022

SUPPORTING CITATIONS

The following references appear in the supplemental information: Cideciyan et al., 2012; Roman et al., 2013; Stone, 2007; Wood et al., 2021.

REFERENCES

Baehr, W., Karan, S., Maeda, T., Luo, D.G., Li, S., Bronson, J.D., Watt, C.B., Yau, K., Frederick, J.M., and Palczewski, K. (2007). The function of guanylate cyclase 1 and guanylate cyclase 2 in rod and cone photoreceptors. J. Biol. Chem. *282*, 8837–8847. https://doi.org/10.1074/jbc.M610369200.

Bouzia, Z., Georgiou, M., Hull, S., Robson, A.G., Fujinami, K., Rotsos, T., Pontikos, N., Arno, G., Webster, A.R., Hardcastle, A.J., et al. (2020). GUCY2D-associated Leber congenital amaurosis: a retrospective natural history study in preparation for trials of novel therapies. Am. J. Ophthalmol. *210*, 59–70. https://doi.org/10.1016/j.ajo.2019.10.019.

Boye, S.E., Boye, S.L., Pang, J., Ryals, R., Everhart, D., Umino, Y., Neeley, A.W., Besharse, J., Barlow, R., and Hauswirth, W.W. (2010). Functional and behavioral restoration of vision by gene therapy in the guanylate cyclase-1 (GC1) knockout mouse. PLoS One *5*, e11306. https://doi.org/10.1371/journal.pone.0011306.

Boye, S.L., Conlon, T., Erger, K., Ryals, R., Neeley, A., Cossette, T., Pang, J., Dyka, F.M., Hauswirth, W.W., and Boye, S.E. (2011). Long-term preservation of cone photoreceptors and restoration of cone function by gene therapy in the guanylate cyclase-1 knockout (GC1KO) mouse. Invest. Ophthalmol. Vis. Sci. *52*, 7098–7108. https://doi.org/10.1167/iovs.11-7867.

Boye, S.L., Peshenko, I.V., Huang, W.C., Min, S.H., McDoom, I., Kay, C.N., Liu, X., Dyka, F.M., Foster, T.C., Umino, Y., et al. (2013). AAV-mediated gene therapy in the guanylate cyclase (RetGC1/RetGC2) double knockout mouse model of Leber congenital amaurosis. Hum. Gene Ther. *24*, 189–202. https://doi.org/10.1089/hum.2012.193.

Boye, S.E. (2014). Insights gained from gene therapy in animal models of retGC1 deficiency. Front. Mol. Neurosci. *7*, 43. https://doi.org/10.3389/fnmol.2014.00043.

Boye, S.E. (2016). A mini-review: animal models of GUCY2D Leber congenital amaurosis (LCA1). Adv. Exp. Med. Biol. *854*, 253–258. https://doi.org/10.1007/978-3-319-17121-0_34.

Cideciyan, A.V., Aleman, T.S., Boye, S.L., Schwartz, S.B., Kaushal, S., Roman, A.J., Pang, J.J., Sumaroka, A., Windsor, E.A.M., Wilson, J.M., et al. (2008). Human gene therapy for RPE65 isomerase deficiency activates the retinoid cycle of vision but with slow rod kinetics. Proc. Natl. Acad. Sci. USA *105*, 15112–15117. https://doi.org/10.1073/pnas.0807027105.

Cideciyan, A.V., Swider, M., Aleman, T.S., Feuer, W.J., Schwartz, S.B., Russell, R.C., Steinberg, J.D., Stone, E.M., and Jacobson, S.G. (2012). Macular function in macular degenerations: repeatability of microperimetry as a potential outcome measure for ABCA4-associated retinopathy trials. Invest. Ophthalmol. Vis. Sci. *53*, 841–852. https://doi.org/10.1167/iovs.11-8415.

Cideciyan, A.V., Roman, A.J., Jacobson, S.G., Yan, B., Pascolini, M., Charng, J., Pajaro, S., and Nirenberg, S. (2016). Developing an outcome measure with high luminance for optogenetics treatment of severe retinal degenerations and for gene therapy of cone diseases. Invest. Ophthalmol. Vis. Sci. *57*, 3211–3221. https://doi.org/10.1167/iovs.16-19586.

Cideciyan, A.V., and Jacobson, S.G. (2019). Leber congenital amaurosis (LCA): potential for improvement of vision. Invest. Ophthalmol. Vis. Sci. *60*, 1680–1695. https://doi.org/10.1167/iovs.19-26672.

Cideciyan, A.V., Krishnan, A.K., Roman, A.J., Sumaroka, A., Swider, M., and Jacobson, S.G. (2021a). Measures of function and structure to determine phenotypic features, natural history, and treatment outcomes in inherited retinal diseases. Annu. Rev. Vis. Sci. *7*, 747–772. https://doi.org/10.1146/annurev-vision-032321-091738.

Cideciyan, A.V., Jacobson, S.G., Ho, A.C., Garafalo, A.V., Roman, A.J., Sumaroka, A., Krishnan, A.K., Swider, M., Schwartz, M.R., and Girach, A. (2021b). Durable vision improvement after a single treatment with antisense oligonucleotide sepofarsen: a case report. Nat. Med. *27*, 785–789. https://doi.org/10.1038/s41591-021-01297-7.

Csaky, K., Ferris, F., 3rd, Chew, E.Y., Nair, P., Cheetham, J.K., and Duncan, J.L. (2017). Report from the NEI/FDA endpoints workshop on age-related macular degeneration and inherited retinal diseases. Invest. Ophthalmol. Vis. Sci. *58*, 3456–3463. https://doi.org/10.1167/iovs.17-22339.

Dizhoor, A.M., Lowe, D.G., Olshevskaya, E.V., Laura, R.P., and Hurley, J.B. (1994). The human photoreceptor membrane guanylyl cyclase, RetGC, is present in outer segments and is regulated by calcium and a soluble activator. Neuron *12*, 1345–1352. https://doi.org/10.1016/0896-6273(94)90449-9.

Dizhoor, A.M., and Peshenko, I.V. (2021). Regulation of retinal membrane guanylyl cyclase (RetGC) by negative calcium feedback and RD3 protein. Pflugers Arch. *473*, 1393–1410. https://doi.org/10.1007/s00424-021-02523-4.

Fain, G.L. (2006). Why photoreceptors die (and why they don't). Bioessays *28*, 344–354. https://doi.org/10.1002/bies.20382.

Ferris, F.L., 3rd, Kassoff, A., Bresnick, G.H., and Bailey, I. (1982). New visual acuity charts for clinical research. Am. J. Ophthalmol. *94*, 91–96. https://doi.org/10.1016/0002-9394(82)90197-0.

Hahn, L.C., Georgiou, M., Almushattat, H., van Schooneveld, M.J., de Carvalho, E.R., Wesseling, N.L., Ten Brink, J.B., Florijn, R.J., Lissenberg-Witte, B.I., Strubbe, I., et al. (2022). The natural history of Leber congenital amaurosis and cone-rod dystrophy associated with variants in the GUCY2D gene. Ophthalmol. Retina *6*, 711–722. https://doi.org/10.1016/j.oret.2022.03.008.

Guérin, C.J., Lewis, G.P., Fisher, S.K., and Anderson, D.H. (1993). Recovery of photoreceptor outer segment length and analysis of membrane assembly rates in regenerating primate photoreceptor outer segments. Invest. Ophthalmol. Vis. Sci. *34*, 175–183.

Jacobson, S.G., Aleman, T.S., Cideciyan, A.V., Sumaroka, A., Schwartz, S.B., Windsor, E.A.M., Traboulsi, E.I., Heon, E., Pittler, S.J., Milam, A.H., et al. (2005). Identifying photoreceptors in blind eyes caused by RPE65 mutations: prerequisite for human gene therapy success. Proc. Natl. Acad. Sci. USA *102*, 6177–6182. https://doi.org/10.1073/pnas.0500646102.

Jacobson, S.G., Cideciyan, A.V., Ratnakaram, R., Heon, E., Schwartz, S.B., Roman, A.J., Peden, M.C., Aleman, T.S., Boye, S.L., Sumaroka, A., et al. (2012). Gene therapy for Leber congenital amaurosis caused by RPE65 mutations: safety and efficacy in 15 children and adults followed up to 3 years. Arch. Ophthalmol. *130*, 9–24. https://doi.org/10.1001/archophthalmol.2011.298.

Jacobson, S.G., Cideciyan, A.V., Peshenko, I.V., Sumaroka, A., Olshevskaya, E.V., Cao, L., Schwartz, S.B., Roman, A.J., Olivares, M.B., Sadigh, S., et al. (2013). Determining consequences of retinal membrane guanylyl cyclase (RetGC1) deficiency in human Leber congenital amaurosis en route to therapy: residual cone-photoreceptor vision correlates with biochemical properties of the mutants. Hum. Mol. Genet. *22*, 168–183. https://doi.org/10.1093/hmg/dds421.

Jacobson, S.G., Cideciyan, A.V., Huang, W.C., Sumaroka, A., Nam, H.J., Sheplock, R., and Schwartz, S.B. (2016). Leber congenital amaurosis: genotypes and retinal structure phenotypes. Adv. Exp. Med. Biol. *854*, 169–175. https://doi.org/10.1007/978-3-319-17121-0_23.

Jacobson, S.G., Cideciyan, A.V., Sumaroka, A., Roman, A.J., Charng, J., Lu, M., Choudhury, S., Schwartz, S.B., Heon, E., Fishman, G.A., and Boye, S.E. (2017). Defining outcomes for clinical trials of Leber congenital amaurosis caused by GUCY2D mutations. Am. J. Ophthalmol. *177*, 44–57. https://doi.org/10.1016/j.ajo.2017.02.003.

Jacobson, S.G., Cideciyan, A.V., Ho, A.C., Peshenko, I.V., Garafalo, A.V., Roman, A.J., Sumaroka, A., Wu, V., Krishnan, A.K., Sheplock, R., et al. (2021). Safety and improved efficacy signals following gene therapy in childhood blindness caused by GUCY2D mutations. iScience *24*, 102409. https://doi.org/10.1016/j.isci.2021.102409.

Karan, S., Zhang, H., Li, S., Frederick, J.M., and Baehr, W. (2008). A model for transport of membrane-associated phototransduction polypeptides in rod and cone photoreceptor inner segments. Vision Res. *48*, 442–452. https://doi.org/10.1016/j.visres.2007.08.020.

Krishnan, A.K., Jacobson, S.G., Roman, A.J., Iyer, B.S., Garafalo, A.V., Héon, E., and Cideciyan, A.V. (2020). Transient pupillary light reflex in CEP290- or NPHP5-associated Leber congenital amaurosis: latency as a potential outcome measure of cone function. Vision Res. *168*, 53–63. https://doi.org/10.1016/j.visres.2020.01.006.

Lamb, T.D. (2022). Photoreceptor physiology and evolution: cellular and molecular basis of rod and cone phototransduction. J. Physiol. https://doi.org/10.1113/JP282058.

Laura, R.P., Dizhoor, A.M., and Hurley, J.B. (1996). The membrane guanylyl cyclase, retinal guanylyl cyclase-1, is activated through its intracellular domain. J. Biol. Chem. *271*, 11646–11651. https://doi.org/10.1074/jbc.271.20.11646.

Liu, Y., Ruoho, A.E., Rao, V.D., and Hurley, J.H. (1997). Catalytic mechanism of the adenylyl and guanylyl cyclases: modeling and mutational analysis. Proc. Natl. Acad. Sci. USA *94*, 13414–13419. https://doi.org/10.1073/pnas.94.25.13414.

Lowe, D.G., Dizhoor, A.M., Liu, K., Gu, Q., Spencer, M., Laura, R., Lu, L., and Hurley, J.B.

(1995). Cloning and expression of a second photoreceptor-specific membrane retina guanylyl cyclase (RetGC), RetGC-2. Proc. Natl. Acad. Sci. USA *92*, 5535–5539. https://doi.org/10.1073/pnas.92.12.5535.

Maguire, A.M., Russell, S., Chung, D.C., Yu, Z.F., Tillman, A., Drack, A.V., Simonelli, F., Leroy, B.P., Reape, K.Z., High, K.A., and Bennett, J. (2021). Durability of voretigene neparvovec for biallelic RPE65-mediated inherited retinal disease: phase 3 results at 3 and 4 years. Ophthalmology *128*, 1460–1468. https://doi.org/10.1016/j.ophtha.2021.03.031.

Mihelec, M., Pearson, R.A., Robbie, S.J., Buch, P.K., Azam, S.A., Bainbridge, J.W.B., Smith, A.J., and Ali, R.R. (2011). Long-term preservation of cones and improvement in visual function following gene therapy in a mouse model of Leber congenital amaurosis caused by guanylate cyclase-1 deficiency. Hum. Gene Ther. *22*, 1179–1190. https://doi.org/10.1089/hum.2011.069.

Naka, K.I., and Rushton, W.A. (1966). S-potentials from luminosity units in the retina of fish (Cyprinidae). J. Physiol. *185*, 587–599. https://doi.org/10.1113/jphysiol.1966.sp008003.

Nork, T.M., Murphy, C.J., Kim, C.B.Y., Ver Hoeve, J.N., Rasmussen, C.A., Miller, P.E., Wabers, H.D., Neider, M.W., Dubielzig, R.R., McCulloh, R.J., and Christian, B.J. (2012). Functional and anatomic consequences of subretinal dosing in the cynomolgus macaque. Arch. Ophthalmol. *130*, 65–75. https://doi.org/10.1001/archophthalmol.2011.295.

Olshevskaya, E.V., Peshenko, I.V., Savchenko, A.B., and Dizhoor, A.M. (2012). Retinal guanylyl cyclase isozyme 1 is the preferential in vivo target for constitutively active GCAP1 mutants causing congenital degeneration of photoreceptors. J. Neurosci. *32*, 7208–7217. https://doi.org/10.1523/JNEUROSCI.0976-12.2012.

Perrault, I., Rozet, J.M., Calvas, P., Gerber, S., Camuzat, A., Dollfus, H., Châtelin, S., Souied, E., Ghazi, I., Leowski, C., et al. (1996). Retinal-specific guanylate cyclase gene mutations in Leber's congenital amaurosis. Nat. Genet. *14*, 461–464. https://doi.org/10.1038/ng1296-461.

Perrault, I., Rozet, J.M., Gerber, S., Ghazi, I., Leowski, C., Ducroq, D., Souied, E., Dufier, J.L., Munnich, A., and Kaplan, J. (1999). Leber congenital amaurosis. Mol. Genet. Metab. *68*, 200–208. https://doi.org/10.1006/mgme.1999.2906.

Peshenko, I.V., Olshevskaya, E.V., Yao, S., Ezzeldin, H.H., Pittler, S.J., and Dizhoor, A.M. (2010). Activation of retinal guanylyl cyclase RetGC1 by GCAP1: stoichiometry of binding and the effect of new LCA-related mutations. Biochemistry *49*, 709–717. https://doi.org/10.1021/bi901495y.

Peshenko, I.V., Olshevskaya, E.V., Savchenko, A.B., Karan, S., Palczewski, K., Baehr, W., and Dizhoor, A.,M. (2011). Enzymatic properties and regulation of the native isozymes of retinal membrane guanylyl cyclase (RetGC) from mouse photoreceptors. Biochemistry *50*, 5590–5600. https://doi.org/10.1021/bi200491b.

Peshenko, I.V., Olshevskaya, E.V., Lim, S., Ames, J.B., and Dizhoor, A.M. (2014). Identification of target binding site in photoreceptor guanylyl cyclase-activating protein 1 (GCAP1). J. Biol. Chem. *289*, 10140–10154. https://doi.org/10.1074/jbc.M113.540716.

Peshenko, I.V., Olshevskaya, E.V., and Dizhoor, A.M. (2015a). Evaluating the role of retinal membrane guanylyl cyclase 1 (RetGC1) domains in binding guanylyl cyclase-activating proteins (GCAPs). J. Biol. Chem. *290*, 6913–6924. https://doi.org/10.1074/jbc.M114.629642.

Peshenko, I.V., Olshevskaya, E.V., and Dizhoor, A.M. (2015b). Dimerization domain of retinal membrane guanylyl cyclase 1 (RetGC1) is an essential part of guanylyl cyclase-activating protein (GCAP) binding interface. J. Biol. Chem. *290*, 19584–19596. https://doi.org/10.1074/jbc.M115.661371.

Peshenko, I.V., Olshevskaya, E.V., and Dizhoor, A.M. (2020). *GUCY2D* mutations in retinal guanylyl cyclase 1 provide biochemical reasons for dominant cone-rod dystrophy but not for stationary night blindness. J. Biol. Chem. *295*, 18301–18315. https://doi.org/10.1074/jbc.RA120.015553.

Roman, A.J., Cideciyan, A.V., Aleman, T.S., and Jacobson, S.G. (2007). Full-field stimulus testing (FST) to quantify visual perception in severely blind candidates for treatment trials. Physiol. Meas. *28*, N51–N56. https://doi.org/10.1088/0967-3334/28/8/N02.

Roman, A.J., Cideciyan, A.V., Schwartz, S.B., Olivares, M.B., Heon, E., and Jacobson, S.G. (2013). Intervisit variability of visual parameters in Leber congenital amaurosis caused by RPE65 mutations. Invest. Ophthalmol. Vis. Sci. *54*, 1378–1383. https://doi.org/10.1167/iovs.12-11341.

Roman, A.J., Cideciyan, A.V., Wu, V., Mascio, A.A., Krishnan, A.K., Garafalo, A.V., and Jacobson, S.G. (2022a). Mobility test to assess functional vision in dark-adapted patients with Leber congenital amaurosis. BMC Ophthalmol. *22*, 266. https://doi.org/10.1186/s12886-022-02475-y.

Roman, A.J., Cideciyan, A.V., Wu, V., Garafalo, A.V., and Jacobson, S.G. (2022b). Full-field stimulus testing: role in the clinic and as an outcome measure in clinical trials of severe childhood retinal disease. Prog. Retin. Eye Res. *87*, 101000. https://doi.org/10.1016/j.preteyeres.2021.101000.

Sato, S., Peshenko, I.V., Olshevskaya, E.V., Kefalov, V.J., and Dizhoor, A.M. (2018). GUCY2D cone-rod dystrophy-6 Is a "phototransduction disease" triggered by abnormal calcium feedback on retinal membrane guanylyl cyclase 1. J. Neurosci. *38*, 2990–3000. https://doi.org/10.1523/JNEUROSCI.2985-17.2018.

Semple-Rowland, S.L., Lee, N.R., Van Hooser, J.P., Palczewski, K., and Baehr, W. (1998). A null mutation in the photoreceptor guanylate cyclase gene causes the retinal degeneration chicken phenotype. Proc. Natl. Acad. Sci. USA *95*, 1271–1276. https://doi.org/10.1073/pnas.95.3.1271.

Sharon, D., Wimberg, H., Kinarty, Y., and Koch, K.W. (2018). Genotype-functional-phenotype correlations in photoreceptor guanylate cyclase (GC-E) encoded by GUCY2D. Prog. Retin. Eye Res. *63*, 69–91. https://doi.org/10.1016/j.preteyeres.2017.10.003.

Stone, E.M. (2007). Leber congenital amaurosis – a model for efficient genetic testing of heterogeneous disorders: LXIV Edward Jackson Memorial Lecture. Am. J. Ophthalmol. *144*, 791–811. https://doi.org/10.1016/j.ajo.2007.08.022.

Sumaroka, A., Garafalo, A.V., Cideciyan, A.V., Charng, J., Roman, A.J., Choi, W., Saxena, S., Aksianiuk, V., Kohl, S., Wissinger, B., and Jacobson, S.G. (2018). Blue cone monochromacy caused by the C203R missense mutation or large deletion mutations. Invest. Ophthalmol. Vis. Sci. *59*, 5762–5772. https://doi.org/10.1167/iovs.18-25280.

Sunness, J.S., Rubin, G.S., Broman, A., Applegate, C.A., Bressler, N.M., and Hawkins, B.S. (2008). Low luminance visual dysfunction as a predictor of subsequent visual acuity loss from geographic atrophy in age-related macular degeneration. Ophthalmology *115*, 1480–1488.e1-2. https://doi.org/10.1016/j.ophtha.2008.03.009.

Ulshafer, R.J., Allen, C., Dawson, W.W., and Wolf, E.D. (1984). Hereditary retinal degeneration in the Rhode Island Red chicken. I. Histology and ERG. Exp. Eye Res. *39*, 125–135. https://doi.org/10.1016/0014-4835(84)90003-4.

Williams, M.L., Coleman, J.E., Haire, S.E., Aleman, T.S., Cideciyan, A.V., Sokal, I., Palczewski, K., Jacobson, S.G., and Semple-Rowland, S.L. (2006). Lentiviral expression of retinal guanylate cyclase-1 (RetGC1) restores vision in an avian model of childhood blindness. PLoS Med. *3*, e201. https://doi.org/10.1371/journal.pmed.0030201.

Wood, L.J., Jolly, J.K., Buckley, T.M., Josan, A.S., and MacLaren, R.E. (2021). Low luminance visual acuity as a clinical measure and clinical trial outcome: a scoping review. Ophthalmic Physiol. Opt. *41*, 213–223. https://doi.org/10.1111/opo.12775.

Wright, A.F., Chakarova, C.F., Abd El-Aziz, M.M., and Bhattacharya, S.S. (2010). Photoreceptor degeneration: genetic and mechanistic dissection of a complex trait. Nat. Rev. Genet. *11*, 273–284. https://doi.org/10.1038/nrg2717.

Yang, R.B., Robinson, S.W., Xiong, W.H., Yau, K.W., Birch, D.G., and Garbers, D.L. (1999). Disruption of a retinal guanylyl cyclase gene leads to cone-specific dystrophy and paradoxical rod behavior. J. Neurosci. *19*, 5889–5897. https://doi.org/10.1523/JNEUROSCI.19-14-05889.1999.

Young, R.W. (1971). The renewal of rod and cone outer segments in the rhesus monkey. J. Cell Biol. *49*, 303–318. https://doi.org/10.1083/jcb.49.2.303.

Zinchuk, V., and Zinchuk, O. (2008). Quantitative colocalization analysis of confocal fluorescence microscopy images. Curr. Protoc. Cell Biol. *Chapter 4*. Unit 4.19. https://doi.org/10.1002/0471143030.cb0419s39.

STAR★METHODS

KEY RESOURCES TABLE

REAGENT or RESOURCE	SOURCE	IDENTIFIER
Antibodies		
Rabbit polyclonal Anti-RETGC1 antibody	Laura et al. (1996)	RRID: AB_2877058
Chemicals, peptides, and recombinant proteins		
Phusion Flash DNA polymerase mixture	Thermo Scientific	Cat.# F-548L
Pierce SuperSignal West Femto chemiluminescence substrate	Thermo Scientific	Cat.f#34096
[α-^{32}P]GTP	Perkin-Elmer	Cat.# BLU006X250UC
FuGENE HD Transfection Reagent	Promega	Cat.#F2311
Critical commercial assays		
DNA Clean and Concentration-5 kit	Zymo Research	Cat.# D4004
Wizard Miniprep kit	Promega	Cat.# A7510
Experimental models: Cell lines		
Human: HEK293 Cells	Fisher Scientific	Cat#. 11625019
Recombinant DNA		
pRCCMV plasmid Vector	Invitrogen	https://tools.thermofisher.com/content/sfs/vectors/prccmv_map.pdf https://www.creative-biogene.com/prc-cmv-item-vet1315-441184.html
pQBIfN3-based Vector	Clontech	https://amp.chemicalbook.com/ChemicalProductProperty_EN_CB7440502.htm?N=Japan
Software and algorithms		
Excel	Microsoft	N/A
R version 3.6.3	R Foundation for Statistical Computing	https://cran.r-project.org
Optovue Software (RTVue v.6.8.0.27)	Optovue, Inc.	N/A
PLR Software (RETIsystem v1017.2.0.6)	Roland Consult Stasche & Finger GmbH	N/A
Olympus FluoView Software	Olympus	FV10-ASW

RESOURCE AVAILABILITY

Lead contact

Requests for additional information should be directed to the lead contact, Samuel G. Jacobson, MD, PhD (sjacobso@pennmedicine.upenn.edu).

Materials availability

All data that were generated are included in the manuscript. This study did not generate any new unique reagents or materials. DNA constructs used in this study for expressing RetGC1 and its LCA mutants are available from Alexander M. Dizhoor, PhD (adizhoor@salus.edu).

Data and code availability

Data: All relevant patient-level data are displayed in the figures. All requests to the lead contact for data will be reviewed to verify whether the request is subject to any intellectual property or confidentiality obligations. Patient-related data may be subject to confidentiality. Any data that can be shared will be released.

Code: This paper does not report original code.

Additional Information: Any additional information required to reanalyze the data reported in this paper is available from the lead contact upon request.

EXPERIMENTAL MODEL AND SUBJECT DETAILS

The subjects studied in this report (P1, male, age 19; and P2, female, age 32) were clinically and molecularly diagnosed to have Leber congenital amaurosis (LCA) caused by biallelic recessive mutations in the *GUCY2D* gene and are part of an ongoing clinical trial of gene therapy (clinicaltrials.gov; NCT03920007). Genotype and subject details are given in Table S1. Each subject received AAV5-*GUCY2D* (highest dose administered in the trial: 300 μL, 3.3×10^{11} vg/mL) as a uniocular subretinal injection in the central retina. The two patients in the current study are not the same as the previously reported patients from the first cohort of this clinical trial (who received the lowest dose in the trial: 300 μL, 3.3×10^{10} vg/mL) (Jacobson et al., 2021). The specific studies described in this report were approved by the Institutional Review Board of the University of Pennsylvania. The tenets of the Declaration of Helsinki were followed and informed consent was obtained from participants. The current set of observations is not intended to be a full clinical trial report; this will be submitted when the trial is completed.

METHOD DETAILS

Spatial vision

Best corrected visual acuity (BCVA) was measured using Early Treatment Diabetic Retinopathy Study methodology (Ferris et al., 1982) scored as the number of letters correctly read after adjusting for distance (4 m or 1 m) and expressed as logarithm of the minimum angle of resolution (logMAR). Low luminance visual acuity (LLVA) methodology was modified from that used in age-related macular degeneration (Sunness et al., 2008). Specifically, back-illuminated tumbling E charts were used in order to reduce learning effects. Eyes were dark-adapted 20 min and testing was performed in a dark room with a 2 log unit neutral density filter intercalated before the refractive lenses in a trial holder. Chromatic grating acuity (CGA) was estimated using a modified MP1 (Cideciyan et al., 2016; Sumaroka et al., 2018). In brief, a modified microperimeter presented incremental red gratings of a range of spatial frequencies and contrasts on a bright blue background (2.2 log phot-Td). A steady grating stimulus of 11° diameter was shown on a steady and uniform background of 32° in diameter. The gratings were oriented at either 45° or 135°, and patients were asked to choose a direction (i.e. two-alternative forced-choice paradigm). Ten trials were shown at each stimulus spatial frequency and the threshold was defined as the highest spatial frequency with at least 90% correct responses.

Full field stimulus testing (FST) – Chromatic, dark-adapted state

Dark-adapted chromatic (blue and red stimuli) FST was performed at baseline and periodically post-treatment (Roman et al., 2007, 2022b).

Mobility in the dark-adapted state

Vertical LED strips on a plane resembling a beaded curtain were programmed to produce a rectangular pattern target defining a 'door' of varying luminance that could appear at one of three positions. The subject began the task at a starting position ~4 m away from the device and was instructed to proceed to touch the door. Success was defined as the subject touching within the 'door' area. The test was performed monocularly in the dark-adapted state and with dilated pupils.

The dimmest scene luminance used was near the absolute functional vision threshold for normal scotopic vision. Mobility performance at different scene illuminations was evaluated using percent success of navigation over a fixed number of trials. The success/not success data at each set (10 trials) of all luminance steps tested were fit individually for each eye by logistic regression with asymptotes of 0.3 and 1.0. The threshold for successful travel was defined as the luminance corresponding to 65% success on the fitted curve (Roman et al., 2022a).

Dark-adapted chromatic perimetry

Sensitivity profiles with chromatic stimuli (500 nm and 650 nm) in the vertical meridian were performed with a modified automated perimeter in the dark-adapted state (Cideciyan et al., 2021a). In brief, 1.7° diameter

200 ms duration stimuli were presented at 2° intervals up to 30° eccentric. Results were compared to normal ranges to determine sensitivity losses in patients, and chromatic sensitivity differences were used to estimate the type of photoreceptors mediating responses at each location. Data were acquired at baseline and on days post-treatment.

Retina-tracking mesopic microperimetry

To better characterize the sensitivity of specific retinal locations, a retina-tracking microperimeter (MP-1S, Nidek, Padova, Italy) was used (Cideciyan et al., 2021a). In brief, eyes were dilated and fully dark-adapted. Testing was performed uniocularly in a dark room with a black curtain blocking any stray light originating from the computer screen on the examiner's side from reaching the subject's eye. White stimuli (max luminance 127 cd.m^{-2}) of Goldman V size (1.7° diameter) and 200 ms duration were presented on a dim red (1 cd.m^{-2}) mesopic background along the superior vertical meridian extending from 1 to 21° eccentric from the fovea at 1° intervals. Fovea-on-OCT software feature was used to lock the test pattern to the anatomical fovea visible on OCT. Thresholds were estimated using the 4–2 staircase strategy. Data were exported, and a 3-point spatial moving average was applied.

Retinal structure - Optical coherence tomography

Cross-sectional imaging using spectral domain optical coherence tomography (OCT) was performed (RTVue-100, Optovue Inc., Fremont, CA; software, RTVue v.6.8.0.27) (Jacobson et al., 2013, 2017). The OCT images were recorded at baseline along the vertical meridian from the superior extramacular retina to the fovea. Measurements were made of the photoreceptor sublaminae: outer nuclear layer (ONL), outer segment (OS) and inner segment (IS) thicknesses. Attention was paid to the location of the peak sensitivity gained after treatment (500 nm, DA, Figure 2A) at 22–24° superior retina for P1 and 8–10° superior retina for P2 (Jacobson et al., 2013, 2017, 2021).

Pupillary light reflex (PLR)

Pupillometric recordings were performed after at least 40 min of binocular dark adaptation (RETIport; Roland Consult Stasche & Finger GmbH, Brandenburg an der Havel, Germany; software, RETIsystem v1017.2.0.6) (Cideciyan et al., 2021a; Krishnan et al., 2020). An infra-red sensitive video camera (uEye, IDS, Obersulm, Germany) acquired videos of the pupil at 30 frames per second, starting from 1 s before the stimulus onset (pre-stimulus baseline) for a total duration of 15 s. Pupil magnification was fixed (cornea to camera distance 0.3 m, 0.05 mm/pixel). Full field light stimuli (1 s in duration) were blue (peak 465 nm) and red (peak 630 nm) spanned the range from −2.1 to +3.9 $\log_{10}$ scot-cd.m^{-2} and -4.1 to +1.9 $\log_{10}$ scot-cd.m^{-2}, respectively. Direct PLR constriction was recorded in the stimulated eye with the contralateral eye double patched. Stimulus presentations progressed from low to high luminance in 1 log steps; inter-stimulus intervals increased with stimulus luminance for up to 2 min to allow recovery of the pupil diameter to fully dark-adapted values measured at the start of the recording session. The pupil boundaries were detected and tracked automatically from the video record by the commercial software (Roland Consult Ver.180917).

Post-acquisition analyses included visual inspection of individual video frames for pupil detection errors (due to blinks or head movements). If possible, detection errors were corrected manually or sections of recording that were affected were excluded from the analysis. Data containing the stimulus parameters, timestamps and pupil diameter were exported. Response amplitude was defined as the difference between baseline pupil diameter and pupil diameter measured at 0.9 s after the stimulus onset. Response amplitudes were plotted as a function of stimulus luminance and fit with hyperbolic ratio equation (Naka and Rushton, 1966) by minimizing the squared error (Excel, Microsoft). In most cases, blue responses were used, exception being the P1 study eye at post-operative visits where response thresholds reached near normal levels and both blue and red stimuli were used to estimate the threshold. PLR amplitude threshold was defined from the fitted luminance-response curves as the dimmest light level that elicited a PLR amplitude of 0.3 mm at 0.9 s; thresholds were estimated for each eye.

Guanylyl cyclase expression and assays

RetGC1 cDNA inserted in a modified pRCCMV plasmid vector (Invitrogen) was re-coded to introduce new restriction endonuclease sites without changing the original protein sequence. The mutations replicating amino acid substitutions in P1 and P2 were then introduced by ligating the corresponding modified

fragments of cDNA, replacing the wild type protein sequence (Peshenko et al., 2020). Wild type RetGC1 and LCA mutants were expressed under the control of CMV promoter in HEK293 cells transfected using calcium phosphate precipitation of the expressing plasmid. The expression constructs harbored the respective RetGC1 cDNA (Lowe et al., 1995) fragments inserted in the HindIII and XbaI sites of the modified vector, from 76 bp upstream of the codon 1 to 269 bp downstream of the translation termination codon, followed by a fragment containing a bovine growth hormone polyadenylation signal of the expression vector. The membrane fractions from the transfected HEK293 cells were isolated using series of centrifugations in isotonic and hypotonic buffers (Peshenko et al., 2010) and the expression of the RetGC1 variants was then verified by Western immunoblotting, probed by a rabbit polyclonal antibody against the catalytic domain of a human RetGC1 (Peshenko et al., 2010). Aliquots of the membranes equalized by the RetGC1 content using Western immunoblotting developed with a Pierce SuperSignal Femto chemiluminescence substrate were reconstituted with 20 μM recombinant human GCAP1, GCAP2 or GCAP3 (Peshenko et al., 2020) in the presence of 2 mM EGTA and 10 mM Mg^{2+} and assayed for guanylyl cyclase activity using [α-^{32}P]GTP as a substrate (Peshenko et al., 2011), followed by thin-layer chromatography of the reaction mixture on polyethylenimine cellulose and liquid scintillation counting of the [^{32}P]cGMP product of the reaction.

For testing co-localization with GCAP1 *in cyto* (Peshenko et al., 2014), HEK293 cells cultured in a Fisher Scientific 4-well LabTekII coverslip chambers were transfected using a Promega FuGene HD reagent with a ~100:1 mixture of the expressing vectors - one coding for a human RetGC1 tagged by mOrange replacing a part of the RetGC1 ECD domain and the other - a Clontech pQBIfN3-based vector coding for a bovine GCAP1 tagged at the C-terminus with enhanced GFP (Peshenko et al., 2015b, 2020). Confocal images were acquired after 48 hours of incubation in 5% CO_2, 37°C, utilizing an Olympus FV1000 Spectral instrument and using the respective 543-nm and 488-nm wavelengths excitation for mOrange and GFP tags in a sequential mode and processed and analyzed using Olympus FluoView FV10-ASW software (Peshenko et al., 2015b). There were no changes to the images other than minor gamma-correction for better clarity in the print. The fluorochromes distribution and co-localization in the cells were quantified using unmodified images.

QUANTIFICATION AND STATISTICAL ANALYSIS

Due to the limited number of subjects, formal statistics were generally not used. The exceptions were the evaluation of interocular symmetry between the eyes of P2 with the use of t-test and evaluation of the correlation between mobility and FST threshold with Pearson's r. Both analyses were performed using the lme4 (version 1.1-27) package from R 3.6.3 (R Foundation for Statistical Computing, Vienna, Austria).

ADDITIONAL RESOURCES

Clinical trial registry number: NCT03920007.

Link to clinicaltrials.gov entry: https://clinicaltrials.gov/ct2/show/NCT03920007.